Supplement of Atmos. Chem. Phys., 15, 411–429, 2015
http://www.atmos-chem-phys.net/15/411/2015/
doi:10.5194/acp-15-411-2015-supplement

Atmospheric Chemistry and Physics Open Access

Supplement of

Understanding high wintertime ozone pollution events in an oil- and natural gas-producing region of the western US

R. Ahmadov et al.

Correspondence to: R. Ahmadov (ravan.ahmadov@noaa.gov)

Understanding high wintertime ozone pollution events in an oil and natural gas producing region of the western U.S.

Supplemental Information

1 Regression slopes in the top-down inventory

Details of the measurements of NO_y and the various VOCs during the winters of 2012 and 2013 at the Horse Pool site are presented in Edwards et al. (2013) and (2014) and the report available at: http://www.deq.utah.gov/locations/U/uintahbasin/studies/UBOS-2013.htm. Most VOC species were determined by GC-MS in 2012, and GC-FID in 2013 as in Gilman et al. (2013). Aromatics and formaldehyde were determined by PTR-MS in both years (de Gouw and Warneke, 2007; Warneke et al., 2011). During 2012 one-minute average NO_y data were determined by catalytic conversion of NO_y over heated gold and chemiluminescence detection of NO (Williams et al., 2009), and in 2013 it was determined by molybdenum conversion and cavity ringdown detection of NO_2 as described in Wild et al. (2014). One minute average CH_4 was determined using a 3-channel Picarro instrument (Peischl et al., 2012).

Linear regressions of NO_y and VOCs with CH_4 are windowed between the hours of 10:00 and 16:00 MST to capture regionally representative conditions within the daytime boundary layers and minimize effects from isolated plumes observed under more stable conditions. Half-hourly resolution VOCs data from both years are included in the regressions. Table S1 summarizes the linear regressions and slopes with respect to CH_4. VOC emissions are dominated by light alkanes on a molar basis with higher correlations ($r^2 > 0.85$) for primary VOCs, and lower correlations for secondary, oxygenated VOCs. The table also gives the recommended assignment of each VOC into the Statewide Air Pollution Research Center (SAPRC-07) photochemical mechanism (Carter, 2010) or the RACM mechanism (Stockwell et al., 1997), which is a basis for the mechanism used in this study. The same lumped hydrocarbon and oxygenated VOC species are emitted in both emission scenarios.

2 Comparison of the meteorological simulations

Figure S3a, b and c show averaged diurnal time series for meteorological variables – temperature, moisture and wind speed measured at Horse Pool during the evaluation time period 29 January–8 February 2013. We also show the wind roses for the same time period for both measurements and model in Fig. S4. The wind roses are provided separately for the nighttime (00:00 – 06:00 MST) and afternoon (12:00 – 18:00 MST) hours to highlight the changes in the wind fields from the night to the afternoon hours at Horse Pool. The wind speed is reasonably well simulated during the daytime (Fig. S3c). However, at nights the model shows stronger easterly winds, whereas the observations indicate lighter winds mostly from east and north-east. The comparisons also show that WRF captures the cold pool conditions with ~2 ^{o}C bias during daytime at Horse Pool (Figure S3a). The stronger katabatic flows at night in the model could be due to the cold temperature bias in the model (Figure S3a and c). It should be noted that as Figure S3c and Figure S4 show, the measured wind speeds at Horse Pool during the stagnation meteorological conditions were quite low.

We also compared PBL height estimates from the model and the observations in order to assess the model's ability to simulate the cold pool and vertical mixing. Using tethersonde measurements of temperature and relative humidity at 3 locations conducted by the NOAA Global Monitoring Division between 29 January and 8 February 2013, PBL heights were estimated from the vertical gradient of virtual potential temperature. The same method was applied to the model output at corresponding times and locations. The results are shown in Fig. S5. The majority of the daytime (09:00-17:00 MST) PBL height values fall within the range of 50-200 m, with a median of all the measurements of 110 m. Although the model simulates the observed range of the mixed layer depth, it has difficulty in capturing the timing of growth and collapse of the PBL observed within the UB (Fig. S5).

3 Time series of observed and model NO_y, CH_4 and toluene for 2013

Figure S6a, b and c show the time series of observed and model simulated NO_y, CH_4 and toluene at Horse Pool during the time period 29 January–22 February 2013. NO_y measurements began after February 4 2013, and the 3 model cases are the same as those shown for O_3 in Fig. 3a and b of the main text. The model case without oil and gas emissions shows negligible toluene and

CH_4 above background specifications, but a noticeable contribution from sources other than the oil and gas sector for NO_y. As discussed in more detail within the main text, on average 57% of the non-oil/gas sector NO_y can be attributed to the mobile sectors of Vernal and Roosevelt, Utah, and surrounding population, with the remaining attributed to the Bonanza power plant. For the top-down and bottom-up emission cases, biases for all three species are apparent, and summarized within Table 3b of the main text. The simulation using the top-down emission case is in better qualitative and quantitative agreement with the observations.

It is important to note that the top-down inventory assumes emissions are constant throughout a diurnal cycle, while the bottom-up NEI-2011 emissions uses diurnal profiles assigned to each SCC (source classification code) contributing to the emissions (version 1 modeling platform, amptpro_for_2011_platform_with_carb_mobile_2011CEM_moves_13aug2013_v0). The UB oil/gas sector non-point inventory has about 20 SCC categories contributing to primary emissions, but a single diurnal profile common to all the major source types. This cycle has a minimum (44% of diurnal average) between 02:00 and 03:00 MST, and a maximum (152% of average) between 14:00 and 15:00 MST. As best shown in Figure S6, all primary emitted species in the bottom-up inventory show a regular peak occurring between 16:00 and 18:00 MST, and a minimum typically occurring between 03:00 am and 06:00 MST. The sharp decrease in primary species for the bottom-up emission scenario mimics the diurnal pattern of O_3 predicted in the top-down emission scenario (main text, Figure 3b). In both cases the model effectively transports Basin wide accumulations down the Green River valley floor, with the compensating katabatic circulation bringing in diluted and cleaner air to the Horse Pool site from up-wind. For the primary emitted species in the top-down emission scenario (with constant diurnal profile) the effect of nighttime dilution on the diurnal profile is significantly reduced but still apparent.

Table S1. Linear regression slope (ppbv/ppmv), standard deviation of fit (StDv (ppbv/ppmv)), r^2 correlation coefficient, VOC species assignments to the SAPRC-07 and RACM chemical mechanisms for 10:00–16:00 MST observations at Horse Pool during the winters of 2012 and 2013.

Chemical species	Slope	StDv	r^2	SAPRC-07 VOC assignment	RACM VOC assignment
NO_y	3.026	0.56	0.6	-	-
Ethane	57.87	1.02	0.9	ALK1	ETH
Propane	26.47	0.38	0.9	ALK2	0.519*HC3
Methanol	9.152	1.67	0.3	MEOH	0.402*HC3
n-butane	8.902	0.23	0.9	ALK3	1.11*HC3
i-butane	5.861	0.16	0.9	ALK3	1.11*HC3
i-pentane	3.897	0.11	0.9	ALK4	0.964*HC5
n-pentane	3.532	0.17	0.9	ALK4	0.964*HC5
2 and 3 methylpentane	2.942	0.21	0.8	ALK4	HC5
1-methyl cyclohexane	2.091	0.03	0.9	ALK5	HC8
n-hexane	1.613	0.06	0.9	ALK4	0.17*HC5+0.83*HC8
Acetone	1.541	0.25	0.7	ACET	0.253*KET
Cyclohexane	1.178	0.01	0.9	ALK5	HC8
1-methyl cyclopentane	0.966	0.02	0.9	ALK4	0.956*HC5
2,2 dimethylbutane	0.863	0.68	0.1	ALK3	0.964*HC3
Acetaldehyde	0.861	0.11	0.7	CCHO	ALD
n-heptane	0.807	0.06	0.8	ALK4	HC5
Toluene	0.758	0.03	0.9	ARO1	TOL
Formaldehyde	0.638	0.06	0.8	HCHO	HCHO
Benzene	0.593	0.00	0.9	0.295*ARO1	0.293*TOL
MEK	0.568	0.09	0.7	MEK	KET
n-octane	0.548	0.02	0.9	ALK5	0.945*HC8
1,3 dimetylcyclohexane	0.386	0.01	0.9	ALK5	HC8
Ethylene	0.353	0.02	0.8	ETHE	OL2
C8 aromatics	0.349	0.02	0.8	ARO2	XYL
n-nonane	0.216	0.01	0.8	ALK5	HC8
Ethanol	0.161	0.09	0.2	ALK3	1.198*HC3
Acetylene	0.146	0.06	0.4	ALK2	0.343*HC3
1,1,3 trimethyhexane	0.086	0.01	0.7	ALK5	HC8
2,2 dimethylpropane	0.085	0.02	0.5	ALK2	0.44*HC3
1,2 dimethylcyclohexane	0.078	0.00	0.9	ALK5	HC8
n-decane	0.075	0.00	0.8	ALK5	HC8
C9 aromatics	0.071	0.01	0.7	.0879*ARO1+.9121*A	.0879*TOL+.9121XY
2,2 dimethylbutane	0.059	0.00	0.9	ALK3	0.964*HC8
Propanal	0.057	0.01	0.5	RCHO	ALD
Ethylbenzene	0.051	0.00	0.9	ARO1	TOL

Ethylcyclohexane	0.049	0.00	0.9	ALK5	HC8
n-undecane	0.046	0.00	0.8	ALK5	HC8
1,3 dimethylcyclohexane	0.043	0.00	0.9	ALK5	HC8
1,2,4 trimethylbenzene	0.040	0.00	0.8	ARO2	XYL
Furan	0.035	0.03	0.0	ARO2	XYL
1,3,5 trimethylbenzene	0.030	0.00	0.8	ARO2	XYL
Naphthalene	0.030	0.00	0.5	ARO2	XYL
Propylene	0.028	0.00	0.7	OLE1	OLT
1-eth,3,4-methylbenzene	0.023	0.00	0.8	ARO2	XYL
C10 aromatics	0.014	0.00	0.7	.061*ARO1+.939*AR	.061*TOL+.939*XY
Hexanal	0.013	0.00	0.3	RCHO	ALD
1,2,3 trimethylbenzene	0.012	0.00	0.8	ARO2	XYL
Butanal	0.009	0.00	0.5	RCHO	ALD
n-propylbenzene	0.007	0.00	0.8	ARO1	TOL
C11 aromatics	0.006	0.00	0.6	.0246*ARO1+.975*A	.0246*TOL+.939*XY
i-propylbenzene	0.005	0.00	0.9	ARO1	TOL
1-eth, 2-methylbenzene	0.005	0.00	0.8	ARO2	XYL
Benzaldehyde	0.004	0.00	0.7	BALD	ALD
Methacrolein	0.004	0.00	0.4	MACR	MACR
MVK	0.004	0.00	0.7	MVK	0.5*KET+0.5*OLT
C12 aromatics	0.003	0.00	0.4	ARO2	XYL
1,3 butadiene	0.002	0.00	0.6	OLE2	OLI
Vinylbenzene	0.002	0.00	0.1	OLE2	TOL
Isoprene	0.000	0.02	0.0	ISOP	ISO

Table S2. WRF-Chem model configuration. Full description of the model options can be found in: http://www2.mmm.ucar.edu/wrf/users/docs/user_guide_V3/contents.html and http://ruc.noaa.gov/wrf/WG11/Users_guide.pdf.

Horizontal resolution	12 and 4 km nested domains
Vertical resolution	60 layers (18 within lowest 500 m)
Meteorological input	North American Mesoscale analysis
Surface layer	Mellor–Yamada–Nakanishi–Niino
Planetary boundary layer	Mellor–Yamada–Nakanishi–Niino level 2.5
Land Surface	Noah Land Surface Model
Microphysics	WRF Single-Moment 5-class
Shortwave and longwave radiation	rapid radiative transfer model for general circulation models
Gas-phase chemistry	RACM_ESRL
Transport of species	advection and vertical mixing
Advection option for chemical variables	Monotonic

Table S3. Statistics for the observed and simulated meteorological variables at Horse Pool, during daytime (09:00 – 17:00 MST) for the two UBWOS campaigns. N- number of used hourly observations, MO – median of observations, *r*- Pearson correlation coefficient, MB – median model-observation bias, RMSE – root mean square error.

Time period	Variable	N	MO	*r*	MB	RMSE
January 31-February 28 2012	Air Temperature	261	3.27 ^{o}C	0.83	-1.66	2.40
	Moisture	261	2.45 g/kg	0.83	0.31 g/kg	0.59 g/kg
	Wind speed	261	1.60 m/s	0.82	0.59	1.89
January 29-February 22 2013	Air Temperature	225	-6.87 ^{o}C	0.57	0.15 ^{o}C	2.93 ^{o}C
	Moisture	225	2.18 g/kg	0.37	-0.07 g/kg	0.55 g/kg
	Wind speed	225	1.21 m/s	0.15	0.00 m/s	0.89 m/s

Figure S1. Terrain distribution in nested WRF-Chem grids; (a) 12 km and (b) 4km resolution domains.

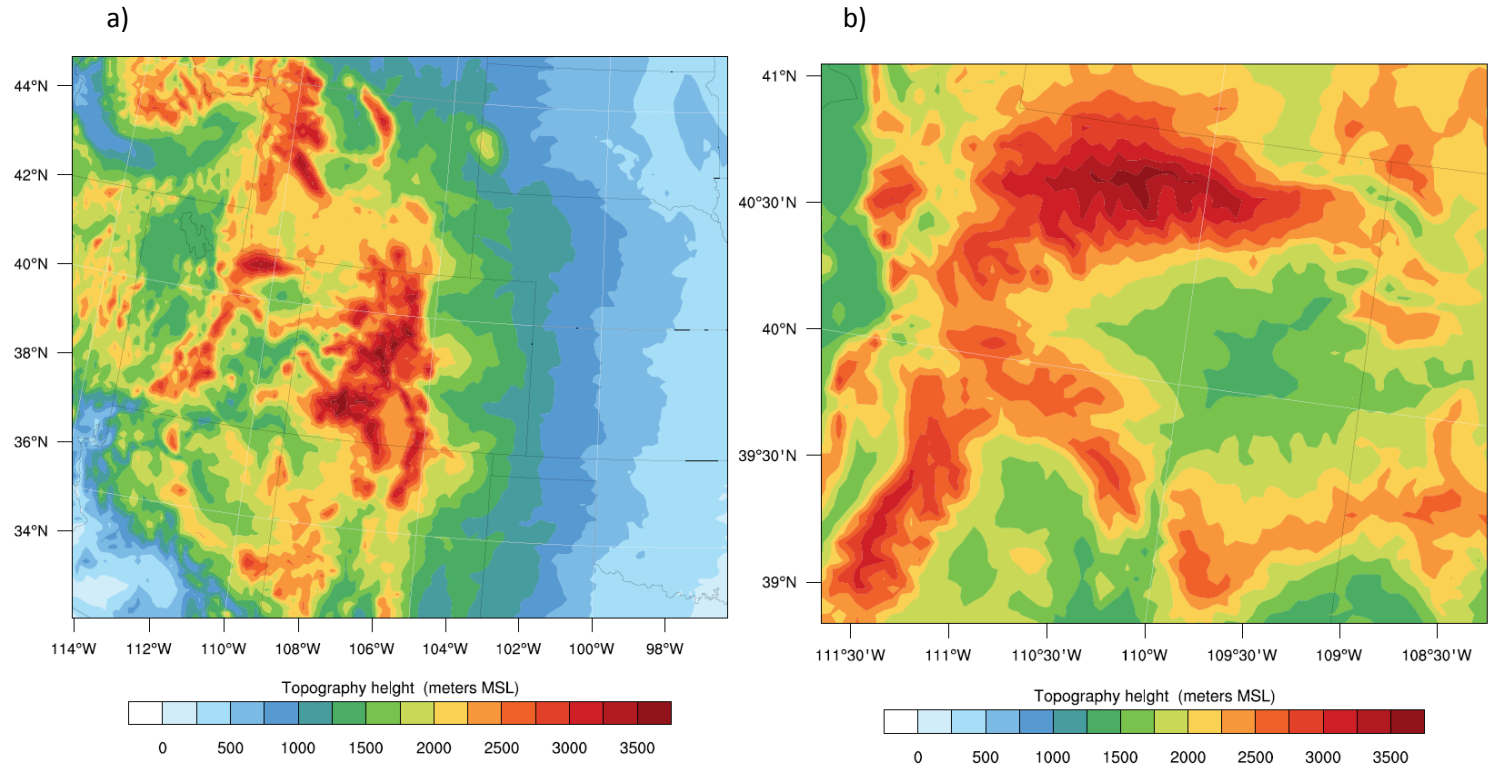

Figure S2. Weather maps from NOAA/HPC (http://www.hpc.ncep.noaa.gov); a) frontal passage, 14:00 MST, 28 January 2013; b) stagnation episode, 14:00 MST, 5 February 2013;

a) b)

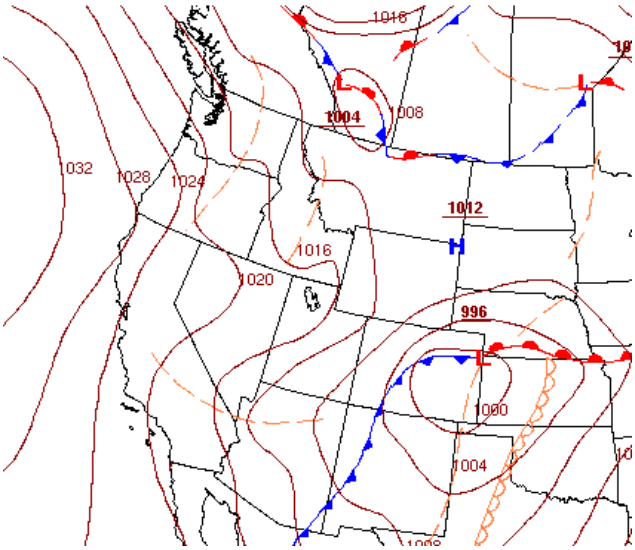

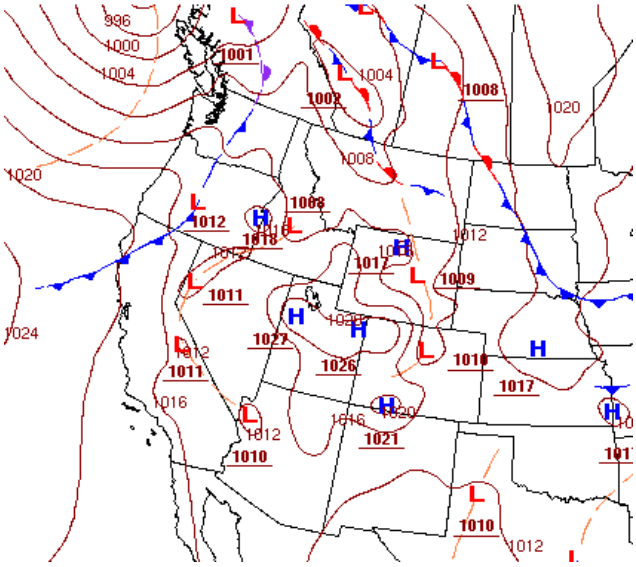

Figure S3. Averaged diurnal cycle of meteorological variables (modeled and measured) during 29 January–8 February 2013. The shaded area on the plots depict the ±σ (standard deviation) of the observed values; (a) Air temperature, (b) water vapor mixing ratio, (c) wind speed.

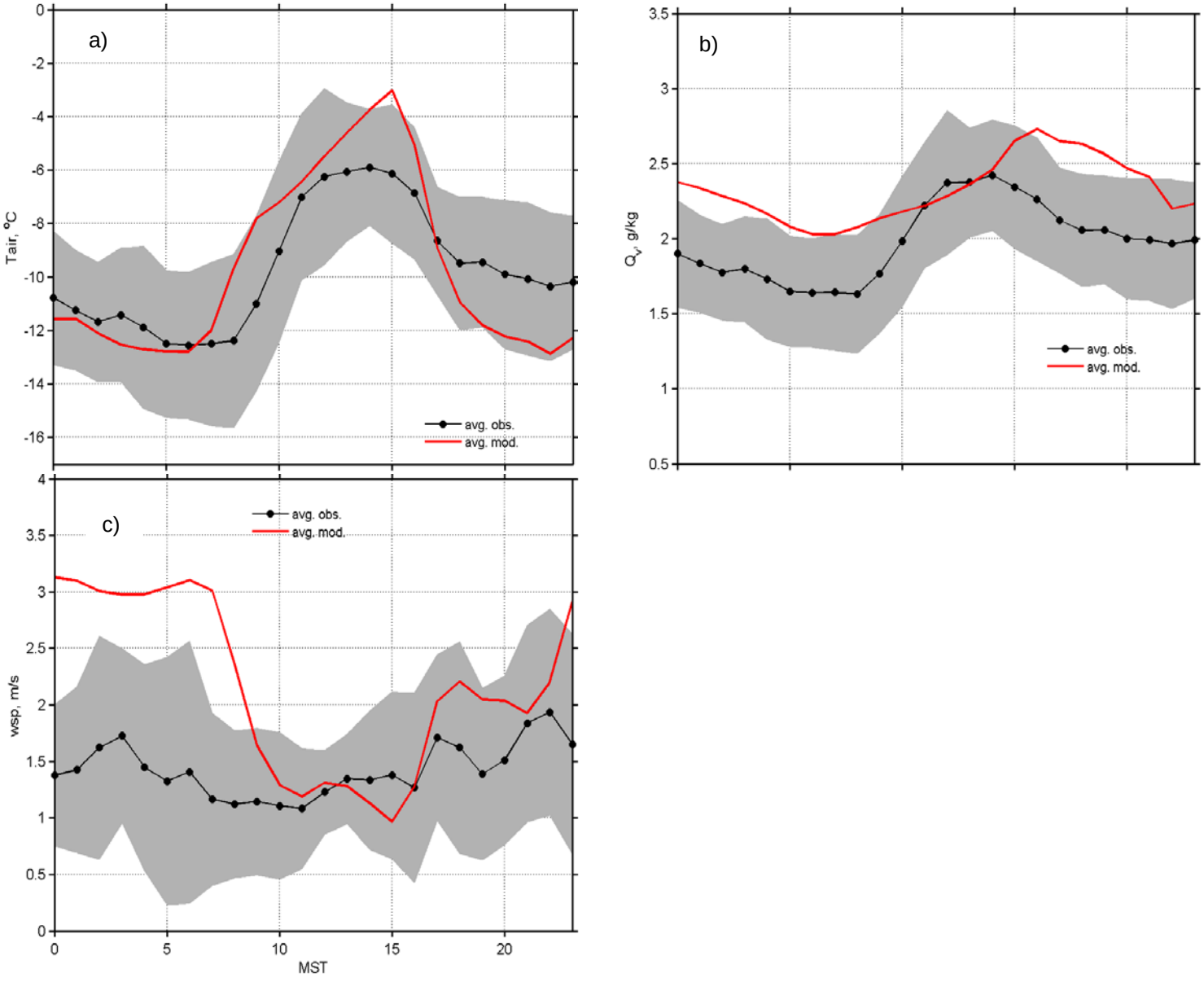

Figure S4. Wind roses showing direction and wind speed from both the measurements and model for 29 January–8 February 2013. The figures on left and right panels correspond to measurements and model results, respectively. The wind roses on the upper and lower rows correspond to nighttime and afternoon hours, respectively.

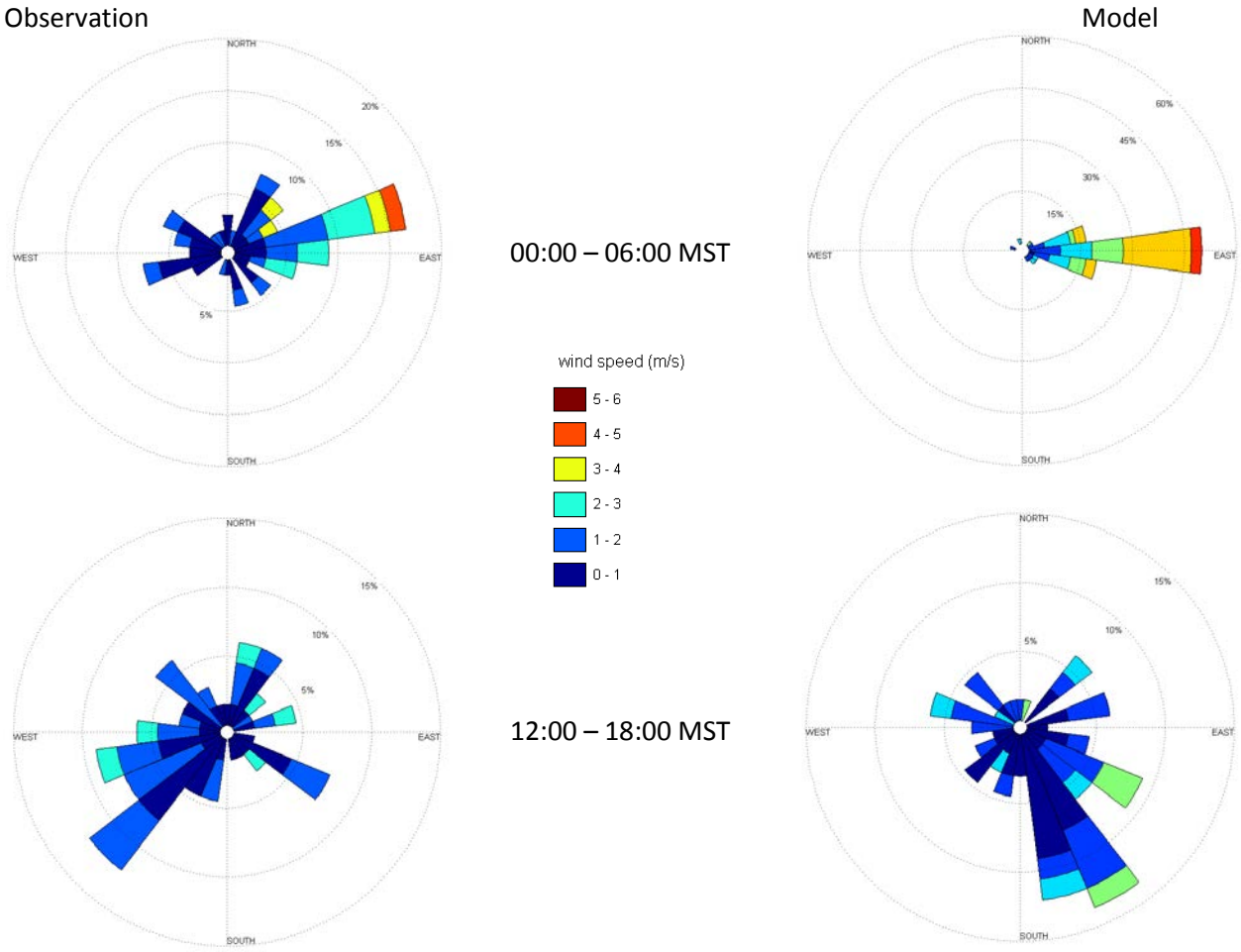

Figure S5. Mixing layer height estimates (3 hourly averaged) determined from vertical profiles of virtual potential temperature from the model output and tethersonde measurements during daytime (09:00 -17:00 MST), 29 January–8 February 2013.

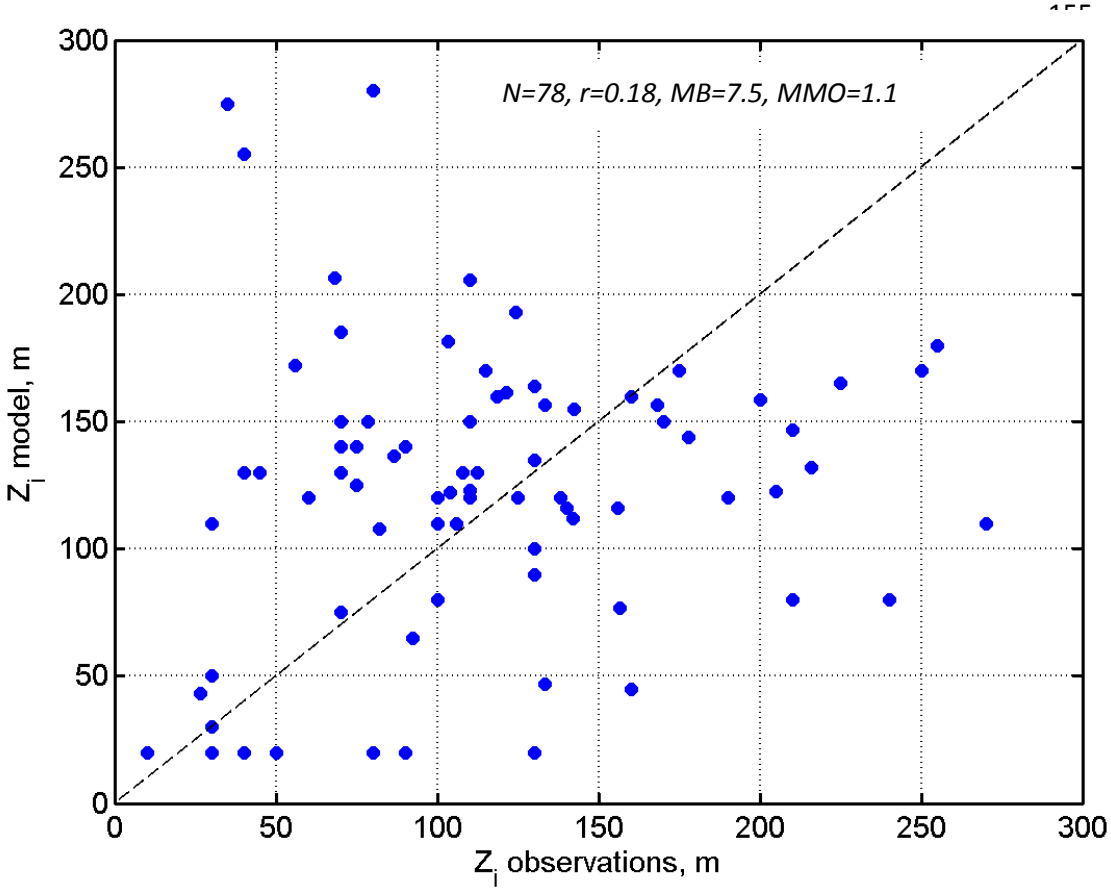

Figure S6. Time series of measured and modeled NO_y, methane (CH_4) and toluene mixing ratios at Horse Pool in January-February, 2013.

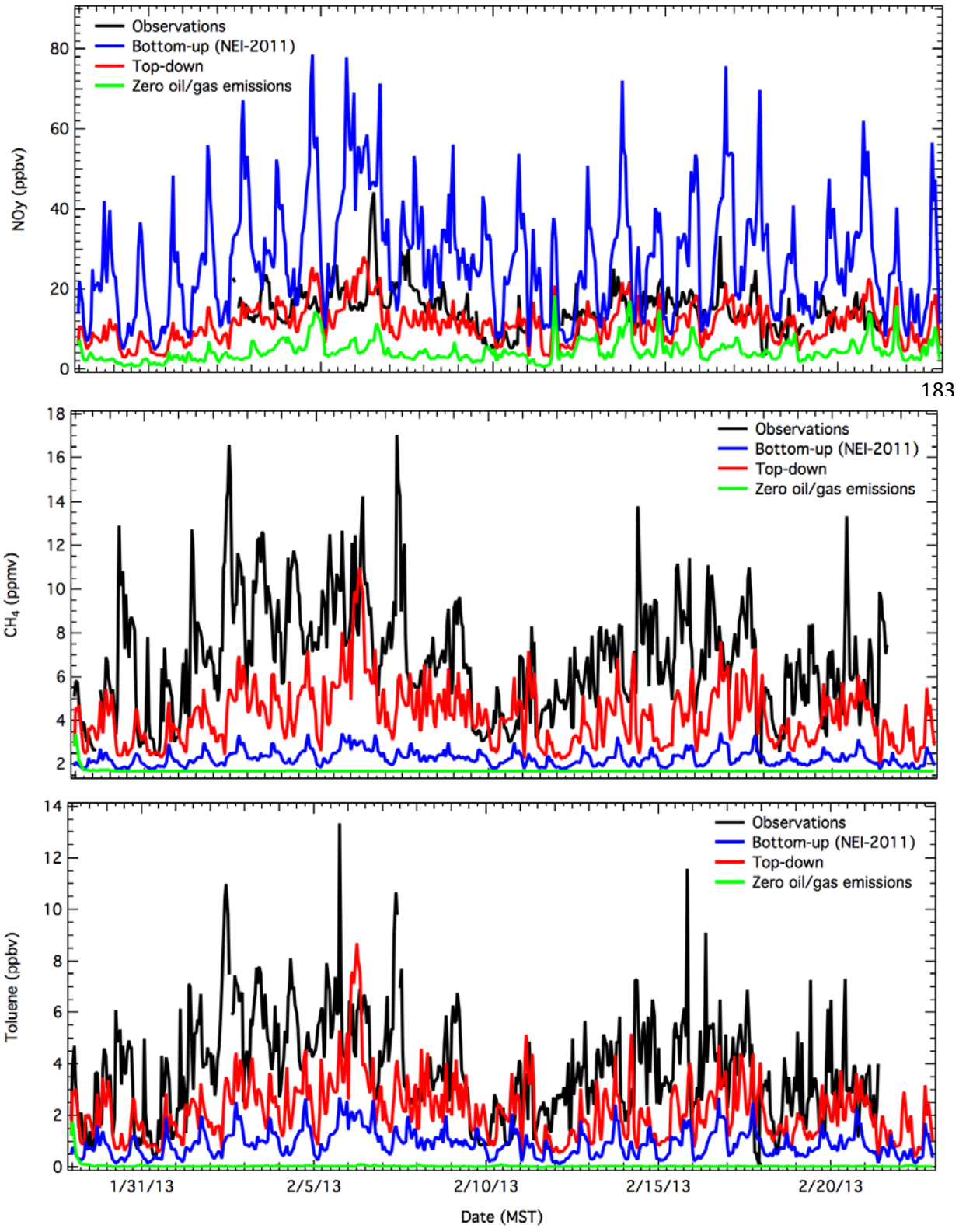

References

Carter, W. P. L.: Development of the SAPRC-07 chemical mechanism, Atmos. Environ., 44, 5324-5335, 10.1016/j.atmosenv.2010.01.026, 2010.

de Gouw, J., and Warneke, C.: Measurements of volatile organic compounds in the earth's atmosphere using proton-transfer-reaction mass spectrometry, Mass Spectrometry Reviews, 26, 223-257, doi:210.1002/mas.20119, 2007.

Edwards, P. M., Young, C. J., Aikin, K., deGouw, J., Dube, W. P., Geiger, F., Gilman, J., Helmig, D., Holloway, J. S., Kercher, J., Lerner, B., Martin, R., McLaren, R., Parrish, D. D., Peischl, J., Roberts, J. M., Ryerson, T. B., Thornton, J., Warneke, C., Williams, E. J., and Brown, S. S.: Ozone photochemistry in an oil and natural gas extraction region during winter: simulations of a snow-free season in the Uintah Basin, Utah, Atmos. Chem. Phys., 13, 8955-8971, 10.5194/acp-13-8955-2013, 2013.

Edwards, P. M., Brown, S., Roberts, J., Ahmadov, R., Banta, R., de Gouw, J., Dubé, W., Field, R., Flynn, J., Gilman, J., Graus, M., Helmig, D., Koss, A., Langford, A., Lefer, B., Lerner, B., Li, R., Li, S., McKeen, S., Murphy, S., Parrish, D., Senff, C., Soltis, J., Stutz, J., Sweeney, C., Thompson, C., Trainer, M., Tsai, C., Veres, P., Washenfelder, R., Warneke, C., Wild, R., Young, C., Yuan, B., Zamora, R.: High winter ozone pollution from carbonyl photolysis in an oil and gas, Nature, 514, 351-354, 2014.

Gilman, J. B., Lerner, B. M., Kuster, W. C., and de Gouw, J. A.: Source Signature of Volatile Organic Compounds from Oil and Natural Gas Operations in Northeastern Colorado, Environ. Sci. Technol., 47, 1297-1305, 10.1021/es304119a, 2013.

Grell, G. A., Peckham, S. E., Schmitz, R., McKeen, S. A., Frost, G., Skamarock, W. C., and 5 Eder, B.: Fully coupled “online” chemistry within the WRF model, Atmos. Environ., 39, 6957–6975, doi:10.1016/j.atmosenv.2005.04.027, 2005.

Peischl, J., Ryerson, T. B., Holloway, J. S., Trainer, M., Andrews, A. E., Atlas, E. L., Blake, D. R., Daube, B. C., Dlugokencky, E. J., Fischer, M. L., Goldstein, A. H., Guha, A., Karl, T., Kofler, J., Kosciuch, E., Misztal, P. K., Perring, A. E., Pollack, I. B., Santoni, G. W., Schwarz, J. P., Spackman, J. R., Wofsy, S. C., and Parrish, D. D.: Airborne observations of methane emissions from rice cultivation in the Sacramento Valley of California, J. Geophys. Res.-Atmos., 117, 10.1029/2012jd017994, 2012.

Stockwell, W. R., Kirchner, F., Kuhn, M., and Seefeld, S.: A new mechanism for regional atmospheric chemistry modeling, J. Geophys. Res.-Atmos., 102, 25847-25879, 1997.

Warneke, C., Veres, P., Holloway, J. S., Stutz, J., Tsai, C., Alvarez, S., Rappenglueck, B., Fehsenfeld, F. C., Graus, M., Gilman, J. B., and de Gouw, J. A.: Airborne formaldehyde measurements using PTR-MS: calibration, humidity dependence, inter-comparison and initial results, Atmos. Meas. Tech., 4, 2345-2358, 10.5194/amt-4-2345-2011, 2011.

Wild, R., Edwards, P., Dube, W., Baumann, K., Edgerton, E., Quinn, P., Roberts, J., Rollins, A., Veres, P., Warneke, C., Williams, E., Yuan, B., Brown, S.: A Measurement of Total Reactive Nitrogen, NOy, together with NO_2, NO, and O_3 via Cavity Ring-down Spectroscopy, Environ. Sci. Technol., 48, 9609-9615, 10.1021/es501896w, 2014.

Williams, E. J., Lerner, B. M., Murphy, P. C., Herndon, S. C., and Zahniser, M. S.: Emissions of NO_x, SO_2, CO, and HCHO from commercial marine shipping during Texas Air Quality Study (TexAQS) 2006, J. Geophys. Res.-Atmos., 114, 10.1029/2009jd012094, 2009.